buildings

MDPI

Article

Optimization of Mix Proportions and Random-Forest-Assisted Exploratory Modeling for Alkali-Activated Fly Ash Geopolymer

Yawei Ma [1,2,*], Xianyang Wang [1], Ying Zhang [1], Binsheng Zhang [1] and Guihong Guo [1,2]

[1] Ministry of Education, Department of Geological Engineering, Lanzhou University, Lanzhou 730000, China
[2] Key Laboratory of Mechanics of Disaster and Environment in Western China, Lanzhou 730000, China
* Correspondence: mayw@lzu.edu.cn

Abstract

Alkali-activated fly ash geopolymers are promising low-carbon binders, but their performance depends strongly on mix proportion design. This study investigated the effects of water-to-binder ratio, sand content, and NaOH concentration on fly ash-based geopolymer using an L25(5^6) orthogonal design. Flexural and compressive strengths were evaluated through range analysis and Analysis of Variance (ANOVA), while Random Forest was used as an exploratory tool for factor-response interpretation. Scanning electron microscopy (SEM), Fourier transform infrared spectroscopy (FTIR), and X-ray diffraction (XRD) were conducted to relate mechanical behavior to microstructural evolution. The optimal combination within the tested levels was a water-to-binder ratio of 0.30, sand content of 40%, and NaOH concentration of 12 mol/L. The maximum flexural and compressive strengths reached 3.65 MPa and 17.98 MPa, respectively. NaOH concentration dominated flexural strength, whereas water-to-binder ratio primarily controlled compressive strength. Model benchmarking and cross-validation showed that the machine-learning results had limited generalization capability under the small-sample condition and should be interpreted as candidate screening rather than independent predictive validation. Microstructural analyses indicated that strength development was associated with matrix densification, aluminosilicate network reorganization, and amorphous geopolymeric gel formation.

Keywords: alkali activation; fly ash; geopolymer; mix proportion optimization; Random Forest; microstructural characterization

1. Introduction

The construction industry faces an urgent imperative to decarbonize, as it accounts for approximately 40% of global resource consumption and over 30% of anthropogenic greenhouse gas emissions. Conventional Portland cement production alone contributes roughly 8% of global CO_2 emissions, driving the search for low-carbon alternatives. Alkali-activated materials, and geopolymers in particular, have emerged as promising candidates because they can be synthesized from industrial solid wastes without high-temperature calcination, reducing energy consumption by up to 60% and carbon emissions by 44–80% compared with ordinary Portland cement [1]. Fly ash, a by-product of coal combustion, represents one of the most abundant aluminosilicate precursors for geopolymer synthesis, with an annual global production exceeding 600 million tonnes and an utilization rate of only about 70%, leaving vast quantities stockpiled and posing environmental hazards.

Geopolymers are inorganic polymers formed by the alkaline activation of aluminosilicate precursors. The term was coined by Davidovits [2] to describe the three-dimensional

Academic Editor: Mijia Yang

Received: 4 June 2026
Revised: 25 June 2026
Accepted: 13 July 2026
Published: 16 July 2026

network of SiO_4 and AlO_4 tetrahedra linked through shared oxygen atoms, resulting in an amorphous to semi-crystalline structure. The mechanical properties of geopolymers are influenced by both the chemical composition of the precursor and the synthesis conditions. While blended systems that combine fly ash with slag or other calcium-rich materials have been extensively studied to achieve high early strength [3,4], pure Class F fly ash geopolymers are often reported to exhibit lower early-age mechanical performance [5]. Nevertheless, pure fly ash systems remain attractive for applications in which low-cost, low-carbon, and durable binders are required, provided that the mix proportion is carefully optimized. Durability is also an important consideration for geopolymer concrete, but mechanical performance remains a basic requirement for practical mix design [6]. In addition to fly ash-based and slag-based systems, other industrial by-products, such as mine tailings and red mud, have also been explored as precursors for geopolymer binders, showing the broader potential of alkali activation in solid-waste utilization [7,8].

The properties of geopolymers are governed by a complex interplay of factors, including the water-to-binder ratio, activator concentration, and aggregate content. The liquid-to-solid ratio controls the availability of the reaction medium and the pore structure of the hardened matrix [9]. The concentration of the alkaline activator, typically sodium hydroxide or sodium silicate, dictates the degree of dissolution of the glassy phase and the subsequent polycondensation rate [10]. The sand content influences the packing density and the interfacial transition zone between the paste and aggregates. Recent studies have highlighted that the optimal range of these parameters is system-specific and can vary substantially depending on the origin and reactivity of the fly ash [11]. Consequently, robust experimental designs and predictive models are essential for systematic optimization.

To navigate the multi-dimensional parameter space efficiently, orthogonal experimental design has been widely adopted as a statistical tool that reduces the number of required trials while preserving the ability to analyze main effects and interactions [12]. However, traditional statistical analysis, such as range analysis and analysis of variance, can only identify factor significance within the tested levels and cannot predict performance at untested combinations. Machine learning techniques offer a powerful complement by modeling complex nonlinear relationships from limited data. Among the various machine learning algorithms, the Random Forest model has gained traction in materials science due to its robustness with small datasets and its capacity to quantify feature importance [13]. Recent research has demonstrated the successful application of Random Forest and other ensemble methods in predicting the mechanical properties of geopolymer concrete, including compressive strength, flexural strength, and modulus of elasticity [14–17]. Nevertheless, a critical gap exists in the current literature: most machine learning-based studies treat the model as a "black box", focusing on prediction accuracy without verifying whether the learned relationships are physically consistent with established geopolymer chemistry and pore structure theory. Moreover, the integration of physically meaningful features, such as the alkali activation index, into machine learning models and the qualitative assessment of their consistency with established geopolymer mechanisms remain insufficiently discussed [17].

This study addresses the above research gap by combining orthogonal experimental design, statistical analysis, Random Forest-assisted exploratory modeling, and microstructural characterization. The effects of water-to-binder ratio, sand content, and NaOH concentration on the flexural and compressive strength of fly ash-based geopolymers were first evaluated using range analysis and ANOVA. A Random Forest model was then developed as an exploratory tool to analyze qualitative factor-response trends, feature importance, and candidate mix proportion regions within the investigated parameter space.

Considering the limited number of independent experimental mixtures, the model results were not treated as fully validated predictions for direct engineering application. Instead, model-derived trends were compared with statistical results and microstructural observations from SEM, FTIR, and XRD to examine their physical consistency. The objective of this study is therefore not to establish a universally generalizable prediction model, but to provide a model-assisted framework for interpreting the coupled effects of mix parameters and identifying candidate proportions for subsequent experimental verification.

2. Experimental

2.1. Raw Material

The fly ash used in this study was supplied by Gansu Bocheng Microsilica Powder Co., Ltd. (Baiyin, China). According to the Chinese standard GB/T 1596-2017 [18], the CaO content of the fly ash was 3.8%, which is below the 10% threshold for Class F fly ash. Therefore, the precursor was classified as Class F fly ash. The main crystalline phases of the fly ash were quartz and mullite, with contents of 59.3 wt% and 36.9 wt%, respectively. The appearance of the raw materials is shown in Figure 1.

Figure 1. Raw Material: (**a**) Fly Ash, (**b**) Sand, (**c**) Na_2SiO_3, and (**d**) NaOH.

In this study, a composite activator solution was prepared using sodium hydroxide(NaOH) solid, sodium silicate (Na_2SiO_3) and tap water. The NaOH solid, with a purity of 99%, was supplied by Shandong Binhua Dongrui Chemical Co., Ltd. Anhydrous sodium silicate granules, having a modulus of 1 (defined as the molar ratio of SiO_2 to Na_2O in $Na_2O{\cdot}SiO_2$), were procured from Henan Borun Casting Materials Co., Ltd. (Figure 1c,d); The fine aggregate used in this experiment was also sourced from Gansu Bocheng Microsilica Powder Co., LTD. The aggregate used in the experiment was characterized by sieve analysis, with the sieve apertures arranged sequentially from top to bottom as follows: 4.75 mm, 2.36 mm, 1.18 mm, 0.6 mm, 0.3 mm, and 0.15 mm. The sand has a fineness modulus of 1.87, classifying it as fine sand. The grading curve of the fine sand is shown in Figure 2.

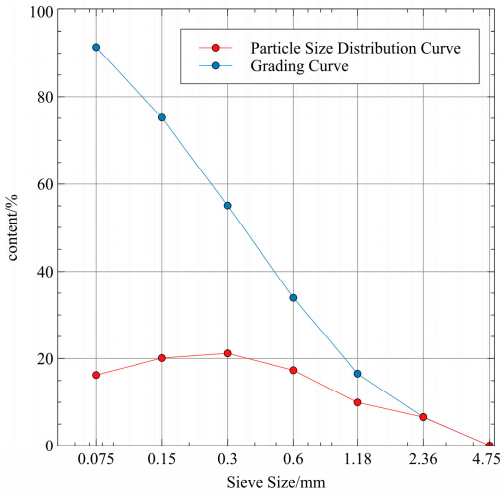

Figure 2. Grading Curve.

2.2. Orthogonal Experimental Design and Geopolymer Preparation Procedure

An $L_{25}(5^6)$ orthogonal array was employed to design the experiments, the specific parameters are shown in Table 1. This design allows for the investigation of up to six factors, each at five levels, through a total of 25 experimental trials. To meet the specific objectives of this study, three key factors—water-to-binder ratio, sand content, and NaOH concentration—were selected, with each factor being systematically examined at five predetermined levels.

Table 1. Factors and Levels for Orthogonal Experiments.

Group No.	Factor 1	Factor 2	Factor 3
	A. Water-to-Binder Ratio	B. Sand Content	C. NaOH Concentration
1	0.25	25%	4 mol/L
2	0.30	30%	6 mol/L
3	0.35	35%	8 mol/L
4	0.40	40%	10 mol/L
5	0.45	45%	12 mol/L

Note: The water-to-binder ratio refers to the mass ratio of total mixing water to fly ash. Sand content refers to the mass ratio of fine sand to fly ash. NaOH concentration refers to the molar concentration of the NaOH solution.

The preparation procedure is summarized in Figure 3. First, fly ash, fine sand, NaOH, sodium silicate, and water were weighed according to the mix design. NaOH and sodium silicate were then added to tap water to prepare the composite alkaline activator. The solution was stirred until the solids were dissolved and then left to cool to room temperature before use. Fly ash and fine sand were placed in the mixer and dry-mixed first. The cooled activator was slowly added to the mixer, and the mixture was stirred until a uniform paste was obtained. The paste was then cast into molds, compacted, sealed, and cured at room temperature for 28 days. After curing, the specimens were demolded and used for mechanical testing.

2.3. Strength Testing and Microstructural Characterization Methods

Flexural strength was measured using a DKZ-5000 (Wuxi Jianyi Instrument & Meter Co., Ltd., Wuxi, China) constant-rate flexural testing machine with a maximum capacity of 5000 N. Compressive strength tests were conducted using a CSS-WAW300DL (Changchun Testing Machine Research Institute Co., Ltd., Changchun, China) electro-hydraulic servo universal testing machine. According to GB/T 17671-2021 [19], the six broken halves obtained from three flexural specimens were used for compressive strength testing. The

loading rate was controlled at 1 cm/min, and both flexural and compressive strengths were calculated from the recorded peak load.

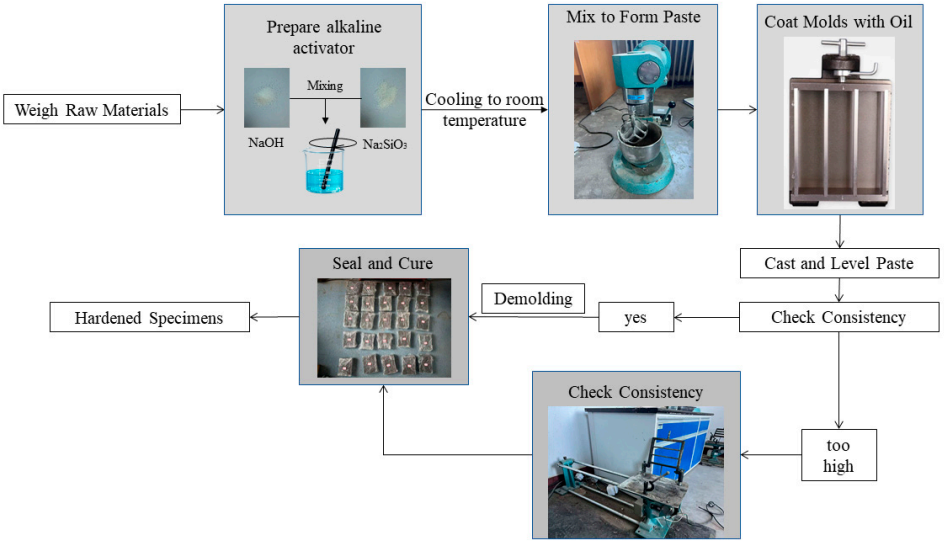

Figure 3. Preparation Flowchart of Fly Ash Geopolymer.

Microstructural characterization was conducted using scanning electron microscopy (SEM), Fourier transform infrared spectroscopy (FTIR), and X-ray diffraction (XRD). SEM observations were performed using a JSM-5600 (JEOL Ltd., Tokyo, Japan) scanning electron microscope under secondary electron imaging mode at an accelerating voltage of 20 kV. The SEM images were collected at magnifications of 500× and 2000× to observe the morphology, pores, microcracks, and gel distribution of the hardened geopolymer matrix. FTIR spectra were collected using a Thermo Scientific Nicolet iS50 FT-IR (Thermo Fisher Scientific, USA) spectrometer over the wavenumber range of approximately 400–4000 cm^{-1} to analyze the evolution of Si–O–T, O–H, and carbonate-related vibration bands. XRD analysis was conducted using an XPERT-PRO X-ray diffractometer (Malvern Panalytical, The Netherlands) with Cu Kα radiation. The generator voltage and tube current were 40 kV and 40 mA, respectively. The scanning range was approximately 15–75° 2θ, with a step size of 0.0083556° under continuous scanning mode.

3. Experimental Data Analysis

3.1. Experimental Data

The results of flexural strength and compressive strength tests for all 25 mix proportions are presented in Table 2. The flexural strength ranged from 0.37 to 3.65 MPa, while the compressive strength ranged from 1.85 to 17.98 MPa.

Table 2. Flexural Strength Test Data and Compressive Strength Experimental Data.

Group No.	f_R/MPa	f_R/MPa	f_R/MPa	$\overline{f_R}$/MPa	$\overline{f_{cu}}$/MPa
$A_1B_1C_1$	0.39	0.36	0.38	0.37	1.85
$A_1B_2C_2$	0.75	0.66	0.61	0.67	3.83
$A_1B_3C_3$	1.09	1.21	1.17	1.16	5.85
$A_1B_4C_4$	1.83	2.29	1.88	2.00	8.72
$A_1B_5C_5$	3.00	3.52	3.21	3.24	14.39
$A_2B_1C_2$	1.90	2.02	2.13	2.02	11.2
$A_2B_2C_3$	1.95	1.99	1.88	1.94	12.88

Table 2. *Cont.*

Group No.	f_R/MPa	f_R/MPa	f_R/MPa	$\overline{f_R}$/MPa	$\overline{f_{cu}}$/MPa
$A_2B_3C_4$	1.76	1.57	1.69	1.67	17.98
$A_2B_4C_5$	3.75	3.40	3.80	3.65	16.98
$A_2B_5C_1$	1.21	0.61	0.75	0.86	6.23
$A_3B_1C_3$	1.27	1.35	1.29	1.30	7.52
$A_3B_2C_4$	2.89	2.98	2.96	2.95	13.69
$A_3B_3C_5$	2.34	2.65	2.55	2.52	14.32
$A_3B_4C_1$	0.80	1.13	1.05	1.09	6.16
$A_3B_5C_2$	1.36	1.08	1.05	1.16	5.84
$A_4B_1C_4$	2.89	3.16	3.45	3.17	9.36
$A_4B_2C_5$	0.96	0.94	0.84	0.91	2.48
$A_4B_3C_1$	0.79	0.77	0.94	0.83	2.26
$A_4B_4C_2$	1.05	0.89	0.94	0.96	3.02
$A_4B_5C_3$	1.03	0.94	1.20	1.05	3.41
$A_5B_1C_5$	0.53	0.56	0.56	0.55	2.5
$A_5B_2C_1$	0.45	0.47	0.52	0.48	2.51
$A_5B_3C_2$	0.64	0.70	0.73	0.69	2.61
$A_5B_4C_3$	0.94	0.87	0.88	0.89	2.88
$A_5B_5C_4$	1.05	1.10	0.96	1.04	3.60

Note: The letter f_R represents flexural strength. The letter $\overline{f_R}$ represents the average flexural strength. The letter $\overline{f_{cu}}$ represents the average compressive strength. Values exceeding the allowable deviation were excluded according to GB/T 17671-2021 before calculating the average strength.

3.2. Flexural Test Calculations

The range analysis of the flexural strength is shown in Table 3.

Table 3. Range Analysis of the Comprehensive Balanced Method for Flexural Strength Results.

Parameters	Factor 1	Factor 2	Factor 3
	A. Water-to-Binder Ratio	B. Sand Content	C. NaOH Concentration
K_1	7.44	7.41	3.63
K_2	10.13	6.95	5.50
K_3	9.02	6.87	6.35
K_4	6.93	8.59	10.82
K_5	3.65	7.36	10.87
k_1	1.49	1.48	0.73
k_2	2.03	1.39	1.10
k_3	1.80	1.37	1.27
k_4	1.39	1.72	2.16
k_5	0.73	1.47	2.17
R	1.30	0.34	1.45

Note: K_i: Sum of test results for each level. Subscript i refers to the i-th factor level. k_i: Mean value of test results for each level. Subscript i refers to the i-th factor level. R: Range, representing the influence degree of each factor.

The variation in K values obtained from the flexural strength range analysis is plotted in Figure 4, providing a visual comparison of the influence of the three factors at different levels.

Based on the comprehensive balanced range analysis method, the optimal values for each condition were determined as follows: water-to-binder ratio of 0.3, sand content of 40%, and NaOH solution concentration of 12 mol/L. The most significant factor affecting flexural strength was the NaOH concentration, followed by the water-to-binder ratio, while sand content exhibited the least influence on flexural strength. The ANOVA results are presented in Table 4.

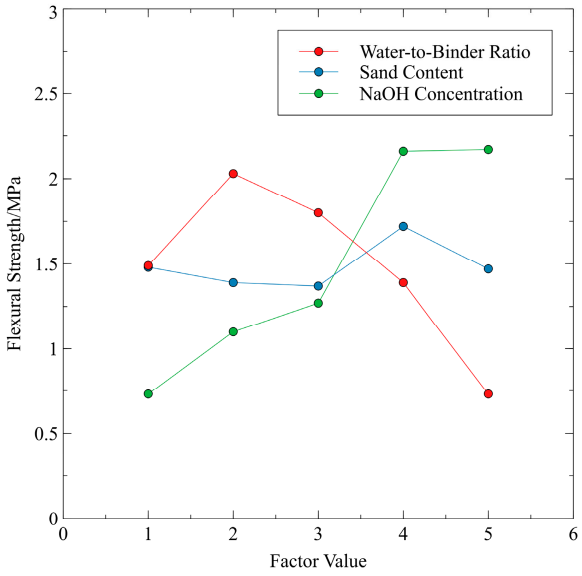

Figure 4. Flexural strength range analysis K value.

Table 4. Analysis of Variance (ANOVA) of Flexural Strength Results.

Source of Variation	Sum of Squares	Degrees of Freedom	Mean Square	F-Value	*p*-Value	Significance
A	4.86	4	1.22	2.39	0.094	Not significant
B	0.38	4	0.095			Pooled into error
C	8.54	4	2.13	4.19	0.017	Significant
D + E + F (Error)	7.77	12	0.65			
B + D + E + F (New Error)	8.15	16	0.51			

Note: B + D + E + F: New error. Because 0.095 is far less than 0.65.

The ANOVA results for flexural strength showed that Factor C, namely NaOH concentration, had a statistically significant effect, with an F-value of 4.19 and a *p*-value of 0.017. In contrast, Factor A, namely the water-to-binder ratio, showed a relatively strong influence trend but did not reach the 0.05 significance level, with an F-value of 2.39 and a *p*-value of 0.094. Factor B, namely sand content, exhibited the smallest contribution and was therefore pooled into the error term. These results indicate that NaOH concentration was the dominant factor controlling flexural strength, followed by the water-to-binder ratio, while sand content had a comparatively limited effect within the investigated range. This conclusion is generally consistent with the range analysis results, where the range values followed the order of NaOH concentration > water-to-binder ratio > sand content.

3.3. Compressive Test Calculations

The range analysis of the compressive strength is shown in Table 5.

Table 5. Range Analysis of Comprehensive Balance Method for Compressive Strength Results.

Parameters	Factor 1	Factor 2	Factor 3
	A. Water-to-Binder Ratio	B. Sand Content	C. NaOH Concentration
K_1	34.64	32.43	19.01
K_2	65.27	35.39	26.5
K_3	47.53	43.02	32.54
K_4	20.53	37.76	53.35
K_5	14.1	33.47	50.67

Table 5. *Cont.*

Parameters	Factor 1	Factor 2	Factor 3
	A. Water-to-Binder Ratio	B. Sand Content	C. NaOH Concentration
k_1	6.928	6.486	3.802
k_2	13.054	7.078	5.3
k_3	9.506	8.604	6.508
k_4	4.106	7.552	10.67
k_5	2.82	6.694	10.134
R	10.234	2.118	6.868

For compressive strength, the corresponding K-value variation is presented in Figure 5. Compared with flexural strength, the water-to-binder ratio exhibited a more pronounced influence on compressive strength.

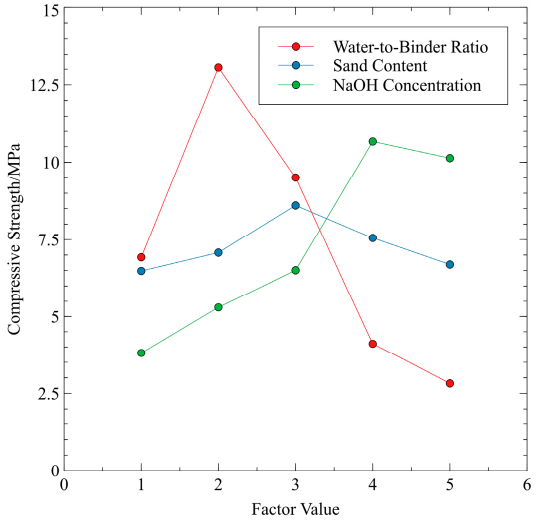

Figure 5. Compressive strength range analysis K value.

Based on the comprehensive balanced range analysis, the optimal combination was determined as a water-to-binder ratio of 0.3, sand content of 40%, and NaOH concentration of 12 mol/L. It was noted that water-to-binder ratio exhibited the most significant influence on compressive strength, followed by NaOH concentration, while sand content showed the least effect. The ANOVA results are presented in Table 6.

Table 6. Analysis of Variance (ANOVA) of Compressive Strength Results.

Source of Variation	Sum of Squares	Degrees of Freedom	Mean Square	F-Value	*p*-Value	Significance
A	341.92	4	85.48	12.51	<0.001	Significant
B	14.21	4	3.55			Pooled into error
C	181.25	4	45.31	6.63	0.002	$p > 0.05$
D + E + F + (Error)	95.13	12	7.93			Significant
B + D + E + F (New + Error)	109.34	16	6.83			

The ANOVA results further confirmed this trend. After pooling the sand content term into the error term due to its relatively small contribution, the water-to-binder ratio showed a statistically significant effect on compressive strength, with an F-value of 12.51 and a *p*-value below 0.001. NaOH concentration also exhibited a significant influence, with an F-value of 6.63 and a *p*-value of 0.002. In contrast, sand content showed a much weaker

contribution and was therefore treated as part of the pooled error term. These results indicate that compressive strength was primarily governed by the water-to-binder ratio, followed by NaOH concentration, while the influence of sand content was comparatively limited within the investigated range.

This result can be explained by the fact that the water-to-binder ratio directly controls the compactness and capillary pore structure of the hardened geopolymer matrix. A relatively low water-to-binder ratio reduces free water content and limits pore formation after hardening, thereby imp-roving compressive strength. NaOH concentration mainly affects the dissolution of the aluminosilicate glass phase in fly ash and the subsequent formation of N-A-S-H gel. Therefore, sufficient alkaline activation is also essential for strength development. However, within the sand content range of 25–45%, the beneficial skeleton effect of sand particles may be partly offset by the dilution of the geopolymer paste, resulting in a relatively weak overall effect on compressive strength.

4. Prediction Using Random Forest (RF) Modeling

4.1. Selection of the RF Model

The general construction procedure of the Random Forest model is schematically illustrated in Figure 6. The model consists of multiple decision trees generated through bootstrap sampling and random feature selection, and the final regression output is obtained by averaging the predictions of individual trees [13].

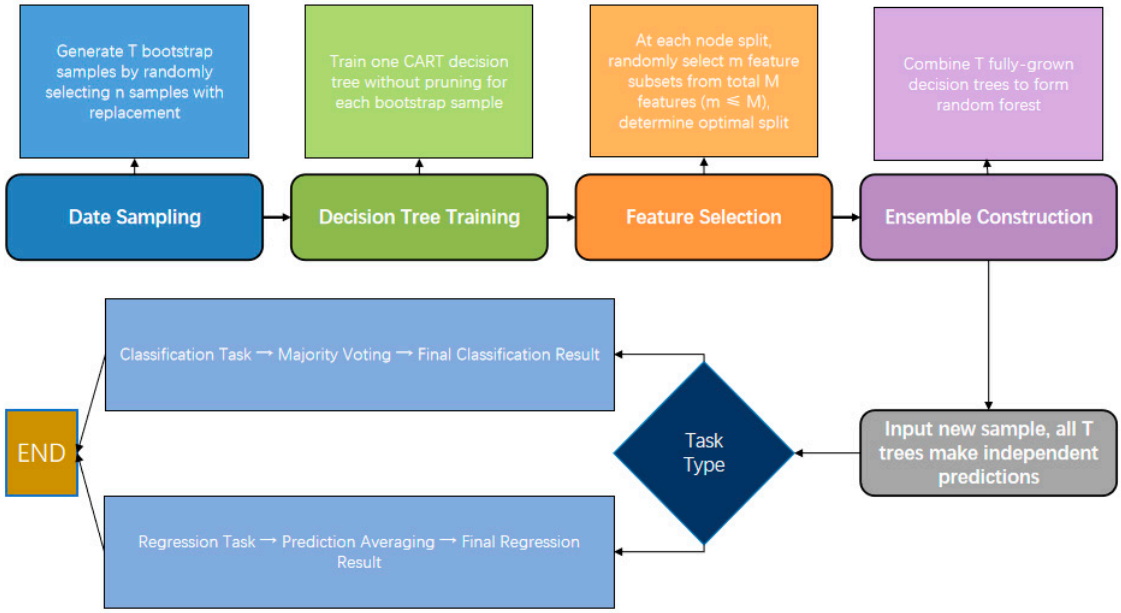

Figure 6. Random Forest Construction Rules Flowchart.

The strength development of geopolymers is governed by nonlinear and heterogeneous effects among precursor characteristics, activator concentration, liquid-to-solid ratio, aggregate content, and curing conditions. Recent reviews have emphasized that machine learning and statistical models can supplement conventional experimental design and empirical regression methods for geopolymer strength prediction, especially when nonlinear factor–response relationships are involved [20]. Therefore, in this study, the Random Forest (RF) algorithm was selected as the baseline machine learning model for exploratory analysis of the mechanical properties of fly ash-based geopolymers.

RF is an ensemble learning method proposed by Breiman [13], in which multiple decision trees are trained using bootstrap samples and random feature selection. For regression tasks, the final prediction is obtained by averaging the outputs of all individual trees:

$$\hat{y} = \frac{1}{N}\sum_{i=1}^{N} T_i(x) \quad (1)$$

where $\hat{y}$ is the predicted value, (N) is the number of decision trees, and $T_i(x)$ represents the output of the (i)-th tree for the input feature vector (x). At each node, the splitting criterion is generally determined by minimizing the mean squared error (MSE):

$$MSE = \frac{1}{n}\sum_{j=1}^{n}\left(y_j - \bar{y}\right)^2 \quad (2)$$

this ensemble structure can reduce the instability of a single decision tree. However, under small-sample conditions, the predictive performance of RF still requires careful evaluation and comparison with alternative algorithms.

The selection of RF was mainly based on three considerations. First, the mechanical performance of geopolymers is governed by nonlinear and coupled effects among the water-to-binder ratio, sand content, and NaOH concentration. Previous studies have shown that machine learning methods are useful for supplementing conventional experimental design and empirical regression models in geopolymer strength prediction, particularly when nonlinear factor–response relationships are involved. Second, RF can provide feature importance scores, which is beneficial for interpreting the relative influence of different mix parameters. Third, compared with a single decision tree, the ensemble structure of RF reduces the instability caused by individual data fluctuations.

Gradient Boosting Machine (GBM), originally formulated by Friedman [21], is also an important ensemble learning algorithm. However, the present study does not assume that RF is universally superior to GBM or other algorithms such as support vector regression, XGBoost, and artificial neural networks. Instead, RF was adopted as a conservative and interpretable baseline model under the current limited experimental data condition. Therefore, the role of RF in this study is mainly to identify qualitative response trends, evaluate relative feature importance, and support model-based virtual screening within the investigated parameter range, rather than to establish a fully generalized prediction model.

4.2. Development and Exploratory Evaluation of the Random Forest Model

Based on the 25 sets of orthogonal experimental data, a systematic data preprocessing pipeline was implemented prior to modeling. First, four categories of derived features were constructed around the three basic mix proportion parameters—water-to-binder ratio, sand content, and NaOH concentration—to expand the feature dimensionality: (1) interaction features, including the pro-duct terms of water-to-binder ratio × NaOH concentration, sand content × NaOH concentration, and water-to-binder ratio × sand content, introduced to capture nonlinear coupling effects among the factors; (2) polynomial features, incorporating the squared terms of the three basic variables t-o characterize possible curvilinear effects of individual factors; (3) physically meaningful features, namely binder content (defined as 1 − sand content), alkali activation index (defined as the ratio of NaOH concentration to water-to-binder ratio), and solid concentration (defined as (1 − water-to-binder ratio) × binder content), all of which carry clear mechanistic implications relevant to the geopolymerization process; (4) composite features, including a water-binder-NaOH composite indicator and a strength potential index, designed to comprehensively reflect the reactivity of the system. In addition, natural logarithmic transformations were applied to

the NaOH concentration and the alkali activation index to capture potential exponential nonlinearities. After the above operations, the initial feature set comprised 16 variables.

To control multicollinearity among the features, the Pearson correlation coefficient matrix of all features was calculated. The results showed that the squared terms were highly correlated with their corresponding linear terms and interaction terms ($|r| > 0.9$), the log-transformed features exhibited strong correlations with their original variables, binder content was perfectly linearly correlated with sand content ($r = -1.0$), and the composite features such as solid concentration were also severely collinear with several original variables. Using a threshold of 0.9, a total of nine redundant features were eliminated. The seven features ultimately retained for modeling were: water-to-binder ratio, sand content, NaOH concentration, the water-to-binder ratio–NaOH concentration interaction, the sand content–NaOH concentration interaction, the water-to-binder ratio–sand content interaction, and the alkali activation index.

Because the original orthogonal experimental program contained only 25 mixtures, a physics-informed perturbation strategy was introduced to support exploratory trend analysis. It should be emphasized that the generated samples were not regarded as independent experimental measurements and were not used as a substitute for external validation. Instead, they were used only to examine whether the model could reproduce physically reasonable local response trends under small variations of the mix parameters.

The perturbations were constrained within the original experimental parameter ranges, namely a water-to-binder ratio of 0.25–0.45, sand content of 25–45%, and NaOH concentration of 4–12 mol/L. Normally distributed perturbations were applied to the original samples, with standard deviations of 0.015 for the water-to-binder ratio, 0.015 for sand content, and 0.3 mol/L for NaOH concentration. The corresponding strength labels were adjusted according to semi-empirical assumptions reflecting the expected influence of water content, alkaline concentration, and aggregate content on geopolymer strength. Random noise was further added to simulate experimental fluctuations, with standard deviations of 0.1 MPa for flexural strength and 0.5 MPa for compressive strength.

After perturbation, the nominal dataset size increased from 25 to 100. However, because the augmented samples were derived from the original experimental data and predefined perturbation rules, they did not introduce new independent experimental information. This issue is particularly important in machine-learning-based scientific studies, where inappropriate data handling may lead to overly optimistic model performance or information leakage [22]. Therefore, all subsequent model-based results should be interpreted as exploratory analyses within the investigated parameter space.

Two independent random forest regression models were developed for flexural strength and compressive strength, respectively. Hyperparameter tuning was conducted via grid search with five-fold cross-validation. The search space covered the number of decision trees (50, 100, 150), maximum tree depth (3, 5, 7, 10), minimum number of samples required to split an internal node (2, 3, 5), minimum number of samples required at a leaf node (1, 2, 3), and the feature sampling strategy at each split ('sqrt', 'log2'), yielding a total of 216 hyperparameter combinations. The optimal configuration determined after 1080 fitting runs was as follows: for the flexural strength model, n_estimators = 50, max_depth = 7, min_samples_split = 2, min_samples_leaf = 2, and ma-x_features = 'sqrt'; for the compressive strength model, n_estimators = 50, max_depth = 5, min_samples_split = 2, min_samples_leaf = 1, and max_features = 'sqrt'. Both models adopted a relatively low number of trees and moderate tree depth, which helped constrain model complexity an d reduce the risk of overfitting on the small dataset.

As shown in Table 7, the RF models exhibited good apparent fitting performance on the augmented dataset, with R^2 values of 0.9537 and 0.9483 for flexural and compres-

sive strength, respectively. The corresponding RMSE and MAE values also indicate that the models could reproduce the response patterns contained in the augmented dataset. However, these values should not be interpreted as independent evidence of generalization performance.

Table 7. Random Forest Model Performance Evaluation Results.

Evaluation Metric	Flexural Strength Model	Compressive Strength Model
Apparent R^2 on augmented dataset	0.9537	0.9483
Apparent RMSE on augmented dataset	0.2107 MPa	1.1516 MPa
Apparent MAE on augmented dataset	0.1493 MPa	0.8095 MPa
Mean relative error	13.88%	13.71%
Five-fold cross-validation R^2	−2.58	−3.07
Model role	Exploratory trend analysis	Exploratory trend analysis

The five-fold cross-validation R^2 values were −2.58 for flexural strength and −3.07 for compressive strength. Negative cross-validation R^2 values indicate that the models performed worse than a simple mean-value predictor on unseen validation subsets. This result reveals the limited generalization capability of the models under the current small-sample condition. Although cross-validation is a standard approach for empirical assessment of predictive performance and hyperparameter tuning, its results should be interpreted carefully when the independent sample size is very small [23].

The poor cross-validation performance can be mainly attributed to the limited number of independent experimental observations. Although the perturbation-based augmentation increased the nominal sample size from 25 to 100, the generated samples were still derived from the original 25 experimental mixtures and predefined semi-empirical rules. Therefore, they cannot substantially increase the independent information content of the dataset.

Accordingly, the RF models developed in this study should not be regarded as fully validated predictive models for direct engineering application. Instead, they are used as exploratory tools to analyze qualitative factor-response trends, estimate relative feature importance, and conduct model-based virtual screening within the experimental parameter space. Independent validation experiments or an enlarged experimental database are still required in future work to improve the generalization capability of the model.

4.3. Benchmarking with Alternative Machine Learning Models

To further justify the selection of Random Forest, a comparative benchmarking analysis was conducted using several commonly adopted machine learning algorithms, including Random Forest (RF), Gradient Boosting Regression (GBR), XGBoost, Support Vector Regression (SVR), and Artificial Neural Network (ANN). These models were selected because they represent different types of nonlinear regression methods and have been widely discussed in machine-learning-based strength prediction studies of geopolymers [20]. GBM was included as a boosting-based ensemble method originally developed by Friedman [21], while XGBoost was further considered as an efficient and regularized tree-boosting algorithm [24].

To ensure a fair comparison, all models were trained and evaluated using the same input features, namely water-to-binder ratio, sand content, NaOH concentration, water-to-binder ratio–NaOH concentration interaction, sand content–NaOH concentration interaction, water-to-binder ratio–sand content interaction, and alkali activation index. The same performance metrics, including coefficient of determination (R^2), root mean square error (RMSE), and mean absolute error (MAE), were adopted for both flexural strength and compressive strength prediction.

Considering the limited number of independent experimental observations, the benchmarking results were interpreted cautiously. The purpose of this comparison was not to claim that a single model achieved universally reliable prediction, but to evaluate whether RF could provide a reasonable balance between fitting performance, model stability, and physical interpretability under the current small-sample condition.

As shown in Table 8, all candidate models produced negative mean cross-validation R^2 values for both flexural and compressive strength prediction. This indicates that, under the current dataset containing only 25 independent experimental mixtures, none of the tested machine learning models achieved satisfactory generalization performance. Therefore, the benchmarking results further confirm the limitation of establishing a fully predictive machine learning model from the present small experimental dataset.

Table 8. Benchmarking results of different machine learning models for strength prediction.

Model	Flexural R^2	Flexural RMSE/MPa	Flexural MAE/MPa	Compressive R^2	Compressive RMSE/MPa	Compressive MAE/MPa	Model Interpretation
RF	−1.084	0.777	0.635	−1.32	3.869	3.291	Interpretable ensemble baseline
GBR	−1.492	0.819	0.678	−0.898	3.496	2.919	Boosting ensemble comparison
XGBoost	−1.336	0.825	0.667	−0.834	3.578	2.947	Regularized tree boosting
SVR	−1.499	0.842	0.628	−0.62	3.465	2.88	Kernel-based nonlinear model
ANN	−5.095	0.952	0.762	−5.785	4.418	3.5	Neural-network nonlinear model

Note: The benchmarking was conducted using the original 25 independent experimental mixtures. The reported values are the mean results of repeated five-fold cross-validation.

For flexural strength prediction, RF showed the least negative R^2 value and the lowest RMSE among the tested models, suggesting relatively better stability for this response variable. However, its R^2 value remained negative, and thus the model should not be interpreted as having reliable predictive accuracy. For compressive strength prediction, SVR achieved the best cross-validation performance, followed by XGBoost and GBR, whereas RF did not provide the best numerical accuracy.

Considering these results, RF was retained as the main model in this study not because it universally outperformed all alternative algorithms, but because it provides feature importance information that can be compared with the range analysis, ANOVA results, and microstructural observations. Therefore, the RF model is used as an interpretable exploratory model for factor-sensitivity analysis and model-assisted virtual screening within the investigated parameter range. The benchmarking results also indicate that future studies should enlarge the experimental database and conduct independent validation before applying machine learning models for engineering prediction.

4.4. Quantitative Analysis of Feature Importance and Factor Influence Patterns

The impurity-reduction-based feature importance method embedded in the Random Forest model was used to evaluate the relative contribution of the seven retained input features. The resulting importance scores for the flexural and compressive strength models are presented in Figure 7.

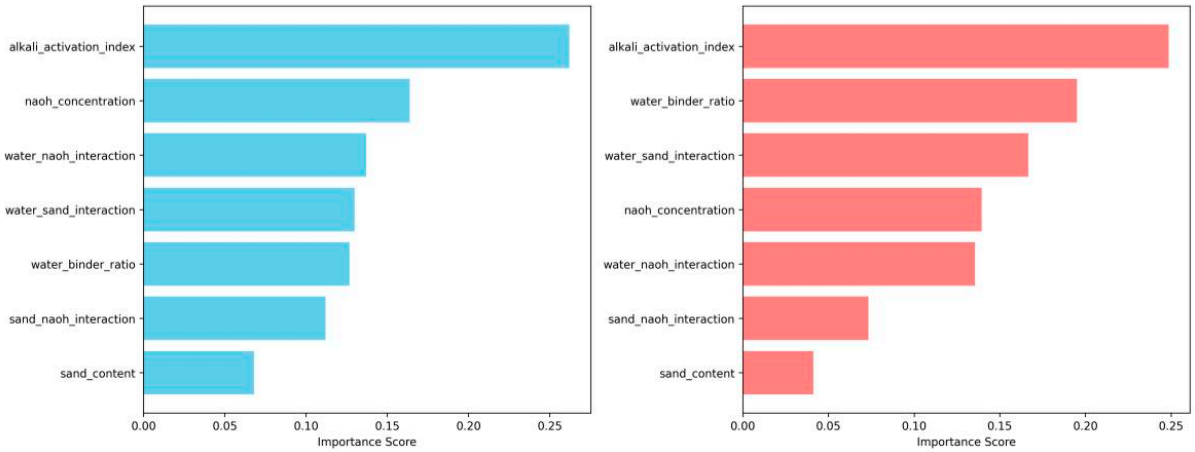

Figure 7. Contribution Weights of the All Key Factors to the Flexural and Compressive Strength of Geopolymer.

The alkali activation index gave the highest importance score in both models, reaching 0.22 for flexural strength and 0.30 for compressive strength. Since this index combines NaOH concentration and water-to-binder ratio, it reflects the combined effect of alkalinity and liquid content. This result is consistent with the basic reaction mechanism of fly ash-based geopolymers, in which water content affects matrix compactness, while NaOH concentration influences aluminosilicate dissolution and gel formation [9,10]. The sand content–NaOH concentration interaction also showed relatively high importance, indicating that the role of fine sand was not completely independent of the alkaline environment.

To compare the three original mix-design parameters more directly, their importance values were extracted from the full feature set and normalized to 100%. The normalized results are given in Figure 8.

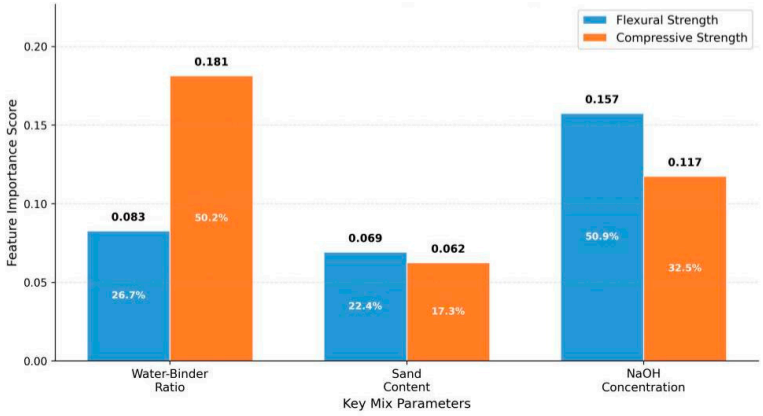

Figure 8. Contribution Weights of the Three Key Factors to the Flexural and Compressive Strength of Geopolymer.

For flexural strength, the normalized contribution followed the order NaOH concentration > water-to-binder ratio > fine sand content, with corresponding values of 50.8%, 26.9%, and 22.3%. This ranking agrees with the range analysis and ANOVA results in Section 3 [12]. For compressive strength, the order changed to water-to-binder ratio > NaOH concentration > fine sand content. The water-to-binder ratio accounted for 56.3% of the normalized contribution, confirming its dominant role in compressive strength development.

The low contribution of fine sand content suggests that, within the range of 25–45%, its skeleton effect may have been partly offset by the dilution of the geopolymer paste [11]. Overall, the feature importance results are consistent with the statistical analysis, but they

should still be understood as exploratory evidence. Given the limited cross-validation performance reported in Table 8, these results do not constitute independent proof of predictive reliability [22,23].

4.5. Multi-Objective Optimization and Three-Factor Coupling Effects

The differential evolution algorithm was applied to search the tested parameter space based on the RF prediction models. Three objectives were considered: flexural strength priority, compressive strength priority, and balanced performance. Since the RF models were built from a limited experimental dataset, the optimized results were used only to suggest possible mix regions, not to replace experimental verification [20,22,23].

For the flexural-strength-priority case, the selected mixture was a water-to-binder ratio of 0.37, fine sand content of 0.26, and NaOH concentration of 10.4 mol/L. The predicted flexural and compressive strengths were 3.64 MPa and 13.66 MPa, respectively. The relatively low sand content increased the proportion of binder matrix, which may be beneficial under bending because the continuity of the hardened paste becomes more important [11].

For the compressive-strength-priority case, the selected mixture was a water-to-binder ratio of 0.31, fine sand content of 0.34, and NaOH concentration of 10.2 mol/L. The predicted compressive strength was 15.44 MPa, while the predicted flexural strength was 2.13 MPa. This result is mainly related to the low water-to-binder ratio, which helps reduce free water and capillary pores after hardening [9].

For balanced performance, the selected mixture was a water-to-binder ratio of 0.31, fine sand content of 0.39, and NaOH concentration of 12.0 mol/L. The predicted flexural and compressive strengths were 3.42 MPa and 15.43 MPa, respectively. This combination kept the matrix relatively dense, provided sufficient alkalinity for aluminosilicate dissolution and gel formation, and maintained a moderate fine sand content for particle packing [25,26].

A Monte Carlo screening was also performed using 1000 randomly generated mixtures within the same parameter range. The distribution of the virtual mixtures is given in Figure 9.

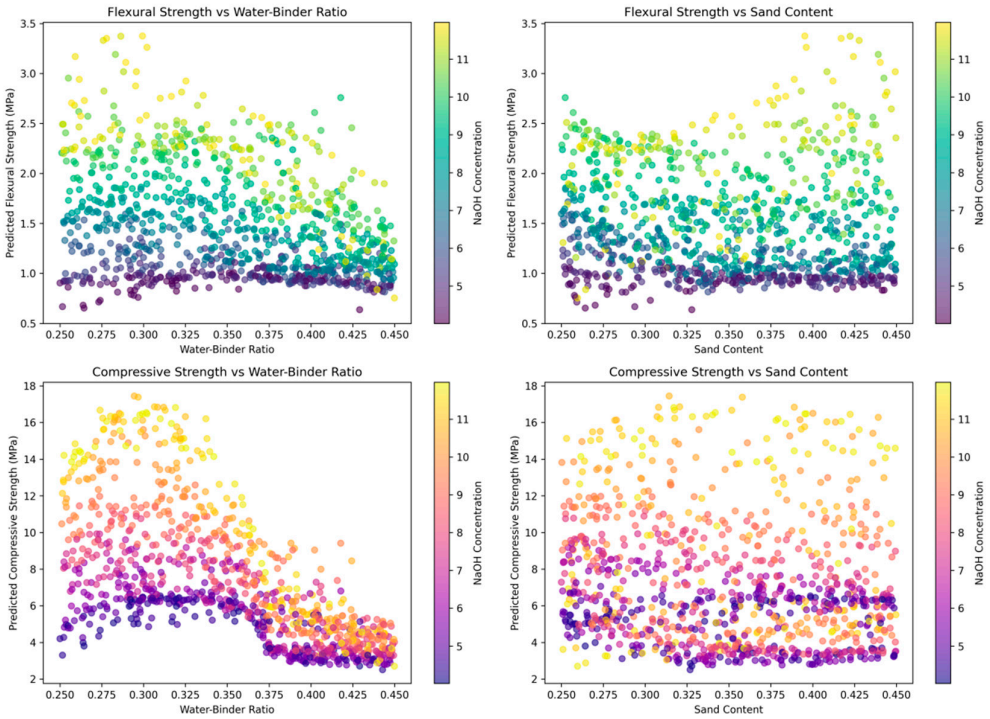

Figure 9. Scatter Plots of the Virtual Experiments.

The best mixture from Monte Carlo screening was located near a water-to-binder ratio of 0.30, fine sand content of 0.40, and NaOH concentration of 11.9 mol/L. The predicted flexural and compressive strengths were 3.37 MPa and 15.06 MPa, respectively. These values were close to the balanced-performance result from differential evolution. However, the two searches were based on the same RF-predicted response surface. Thus, the agreement between them should be regarded as a consistency check within the model, rather than experimental validation [22,23]. The range around a water-to-binder ratio of 0.30–0.31, fine sand content of 0.39–0.40, and NaOH concentration close to 12 mol/L was therefore selected as the candidate region for further testing.

4.6. Physical Consistency Analysis of Model-Predicted Trends

After identifying the candidate mix-proportion region through RF-assisted optimization, it was necessary to examine whether the predicted response trends were physically reasonable within the tested parameter space. Therefore, single-factor sensitivity analysis was conducted by fixing two parameters at their baseline levels and varying the remaining parameter individually. The resulting response curves are presented in Figure 10.

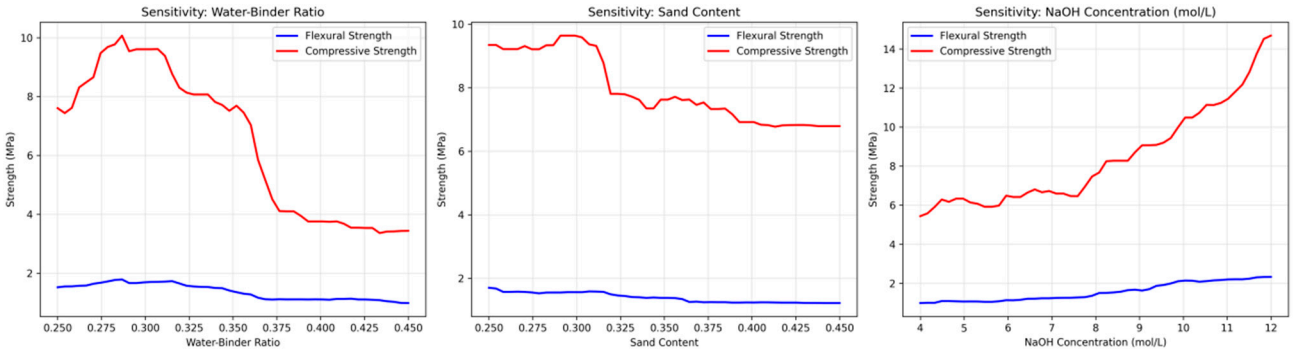

Figure 10. Sensitivity Analysis Curves for the Three Factors.

The sensitivity curves indicate that the model-predicted strength responses were generally consistent with the basic mechanisms of fly ash-based geopolymer strength development. An increase in the water-to-binder ratio tended to reduce strength, which can be attributed to the increase in capillary porosity and the weakening of matrix compactness caused by excessive water [9]. In contrast, increasing NaOH concentration promoted strength development within the investigated range, mainly because higher alkalinity enhanced the dissolution of aluminosilicate species and facilitated the formation of N-A-S-H gel [10]. Sand content showed a relatively limited influence, suggesting that the skeleton effect of fine sand and the dilution effect of the geopolymer paste may have partly offset each other within the range of 25–45%.

These results support the physical plausibility of the RF-derived trends, but they should not be taken as independent model validation. Considering the limited cross-validation performance, the RF results are better interpreted as exploratory trend information and candidate mix-proportion screening. Additional experiments are still needed before the model-assisted optimization results can be used for engineering prediction [22,23].

5. Microstructural Characterization and Mechanistic Interpretation

5.1. SEM Analysis

A total of ten materials were selected for microstructural characterization, including raw fly ash and nine geopolymer specimens. The geopolymer specimens included samples with different water-to-binder ratios at a fixed NaOH concentration of 10 mol/L and samples with different NaOH concentrations at a fixed water-to-binder ratio of 0.30. SEM

was used to observe the morphology, pore structure, microcracks, and gel distribution of the hardened geopolymer matrix. The SEM micrographs of specimens prepared with different water-to-binder ratios are presented in Figure 11.

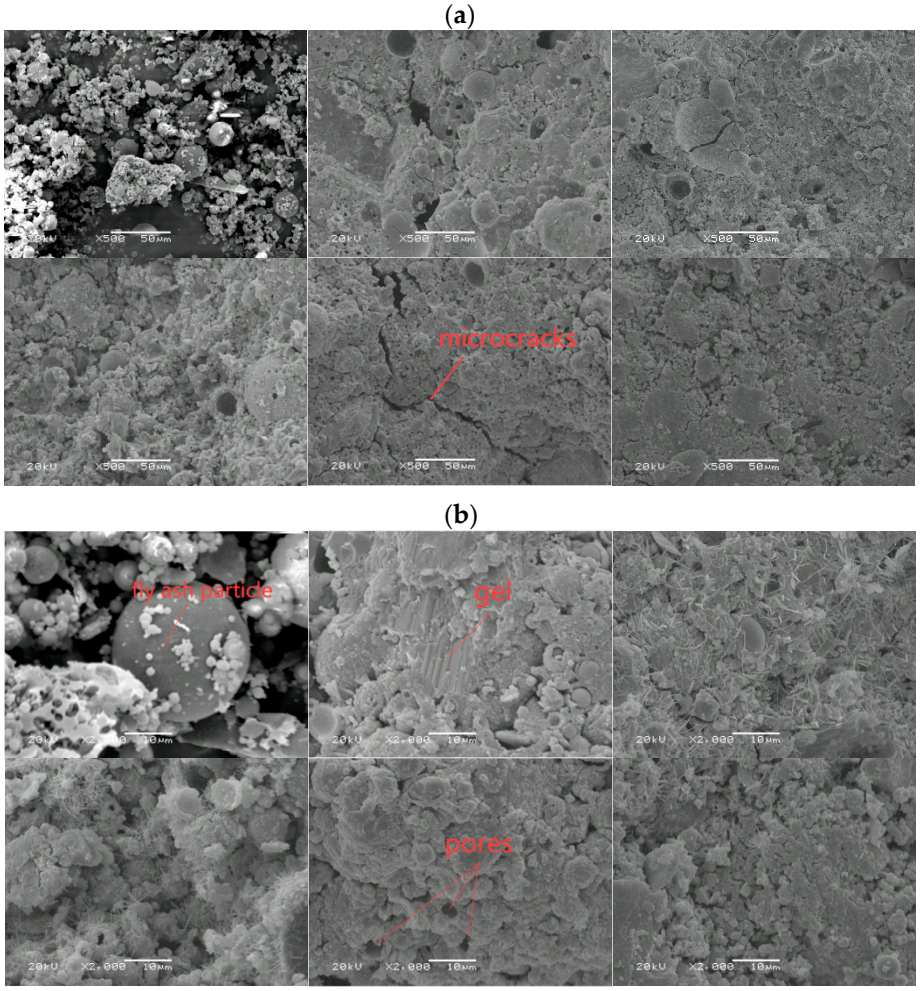

Figure 11. SEM Micrographs of Geopolymers with Fixed NaOH concentration and Different Water-Binder Ratios at Various Magnifications: (**a**) ×500 and (**b**) ×2000.

The SEM micrographs of specimens prepared with different water-to-binder ratios under a fixed NaOH concentration of 10 mol/L. The raw fly ash particles mainly exhibited spherical or near-spherical morphology with relatively smooth surfaces, which is consistent with the typical morphology of Class F fly ash reported in alkali-activated fly ash systems. After alkali activation, part of the fly ash particles remained unreacted, while newly formed gel products were observed around and between the particles. These gel products gradually connected the particles and formed a denser binder matrix, indicating the development of geopolymeric reaction products [25,27].

It should be emphasized that SEM observations mainly provide morphological information. Therefore, the identification of crystalline phases such as quartz and mullite should not be based solely on SEM morphology, but should be interpreted together with the XRD results. In this study, SEM was mainly used to observe particle morphology, matrix compactness, gel formation, pores, and microcracks, while phase identification was supported by XRD analysis [27,28].

With increasing water-to-binder ratio, the matrix morphology changed noticeably. At relatively low to moderate water-to-binder ratios, the gel phase filled part of the interparticle voids, and the matrix appeared comparatively compact. However, when the water-to-

binder ratio became too high, more visible pores and microcracks appeared in the matrix. This indicates that excessive water may increase capillary porosity after hardening and weaken the continuity of the geopolymer matrix [9,11,25]. This observation is consistent with the mechanical results, where the water-to-binder ratio was identified as the dominant factor affecting compressive strength.

Figure 12 presents the SEM micrographs of specimens prepared with different NaOH concentrations at a fixed water-to-binder ratio of 0.30.

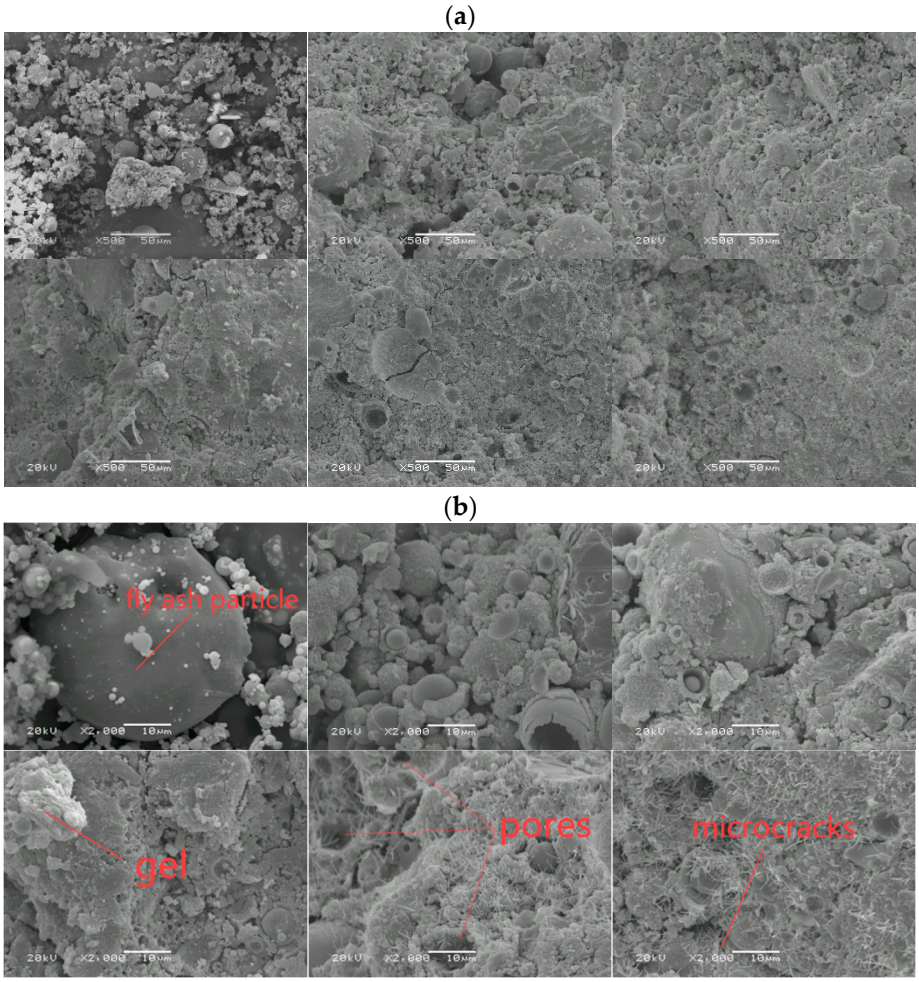

Figure 12. SEM Micrographs of Geopolymers with Fixed Water-Binder Ratios and Different NaOH concentration at Various Magnifications: (**a**) ×500 and (**b**) ×2000.

At lower NaOH concentrations, more unreacted fly ash particles and a less continuous gel phase were observed, indicating insufficient dissolution of the aluminosilicate precursor. With increasing NaOH concentration, the matrix became denser, and more gel products were formed around the particles. This suggests that higher alkalinity promoted the dissolution of fly ash and the formation of geopolymeric gel, thereby improving the mechanical performance [10,25–27]. Overall, the SEM results indicate that strength development is closely related to matrix densification, gel formation, and the reduction in visible defects.

5.2. FTIR Analysis

FTIR analysis was conducted to examine the structural evolution of the aluminosilicate framework during alkali activation. Figure 13 shows the FTIR spectra of raw fly ash and geopolymer specimens prepared under different water-to-binder ratios and NaOH concentrations.

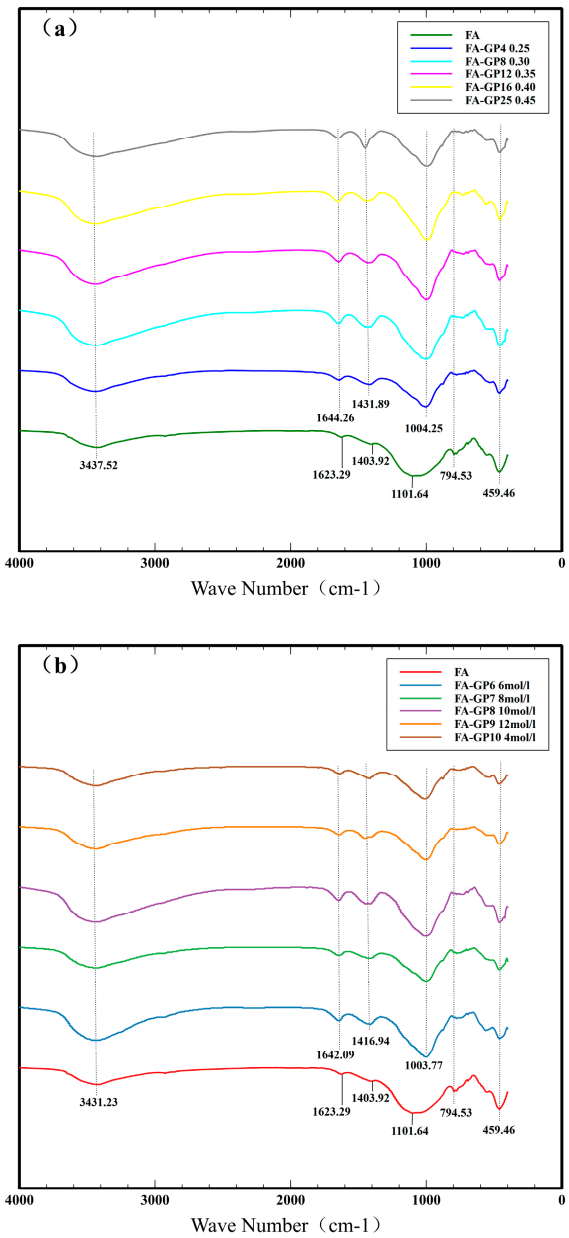

Figure 13. FTIR spectra of fly ash and geopolymer. (**a**) Different water-to-binder ratios at the same NaOH concentration. (**b**) Different NaOH concentrations at the same water-to-binder ratio.

FTIR analysis was conducted to examine the structural evolution of the aluminosilicate framework during alkali activation. The FTIR spectra of raw fly ash and geopolymer specimens prepared under different water-to-binder ratios and NaOH concentrations. The absorption region between 400 and 1200 cm^{-1} is associated with the vibration of Si–O and Al–O bonds and can reflect the structural changes in the aluminosilicate network [25,27,28].

Compared with raw fly ash, the geopolymer samples showed a shift of the main Si–O–T band toward lower wavenumbers. This shift suggests the depolymerization of the original fly ash glass phase and the formation of new Si–O–Al linkages in the geopolymeric gel. The broad bands near 3400 cm^{-1} and 1640 cm^{-1} were related to O–H stretching and bending vibrations, indicating the presence of bound water or hydroxyl-containing species in the reaction products [25,28].

The spectra also reflected the influence of the mix parameters. At relatively low to moderate water-to-binder ratios, the Si–O–T band became more distinct, suggesting a denser aluminosilicate network. In contrast, excessive water may dilute the alkaline

environment and increase pore formation after hardening, which is consistent with the reduction in compressive strength at high water-to-binder ratios. With increasing NaOH concentration, the main Si–O–T band became stronger and shifted more clearly, indicating enhanced dissolution and reorganization of aluminosilicate species. This trend agrees with the mechanical results, where NaOH concentration showed a positive contribution to strength development [10,26,27].

In addition, carbonate-related bands were observed in some specimens, which may be associated with carbonation reactions under highly alkaline conditions. Overall, the FTIR results indicate that a relatively low water-to-binder ratio and sufficient NaOH concentration are beneficial for the formation of a denser geopolymeric network. These findings provide microstructural support for the strength trends observed in the mechanical tests.

5.3. XRD Analysis

XRD analysis was used to examine the crystalline phases and amorphous characteristics of the raw fly ash and geopolymer samples. Figure 14 shows the XRD patterns of raw fly ash and geopolymer samples prepared under different water-to-binder ratios and NaOH concentrations.

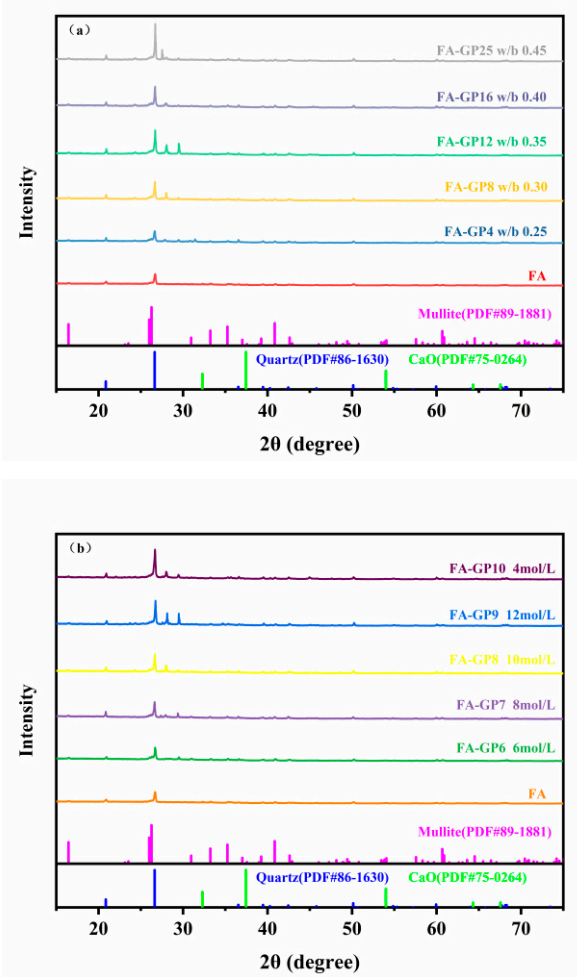

Figure 14. XRD of fly ash and geopolymer. (**a**) Different water-to-binder ratios at the same NaOH concentration. (**b**) Different NaOH concentrations at the same water-to-binder ratio.

XRD analysis was used to examine the crystalline phases and amorphous characteristics of the raw fly ash and geopolymer samples. The raw fly ash mainly contained quartz and mullite as crystalline phases. The characteristic peaks of quartz were mainly observed near 2θ = 26–27°, while mullite showed several diffraction peaks in the ranges

of approximately 16–17°, 26–27°, and 40–42°. In addition, a broad hump in the range of 2θ = 20–35° indicated the presence of an amorphous aluminosilicate glass phase, which is the main reactive component during alkali activation [11,25,27,29].

After alkali activation, the diffraction peaks of quartz and mullite were still present, indicating that these crystalline phases largely remained as relatively stable residual phases. Meanwhile, the broad amorphous hump became more apparent in the geopolymer samples, suggesting the formation of amorphous geopolymeric gel products [25–28]. This result is consistent with the SEM observation of gel products surrounding fly ash particles and the FTIR evidence of aluminosilicate network rearrangement.

The XRD patterns also reflected the effects of water-to-binder ratio and NaOH concentration. At relatively low to moderate water-to-binder ratios, the amorphous hump was more evident, suggesting more favorable gel formation and a denser reaction product structure. When the water-to-binder ratio was too high, the reaction products appeared less compact, which may be associated with dilution of the alkaline environment and increased pore formation [9,11,25]. With increasing NaOH concentration, the amorphous hump became more pronounced, indicating that stronger alkalinity promoted the dissolution of the fly ash glass phase and the formation of geopolymeric gel.

Overall, the XRD results support the conclusion that the mechanical performance of the fly ash-based geopolymer is closely related to the transformation of the amorphous aluminosilicate phase and the formation of geopolymeric gel. However, the XRD results should be interpreted together with SEM and FTIR observations, rather than as independent proof of complete geopolymerization. The combined microstructural evidence indicates that the improved strength performance is mainly associated with matrix densification, enhanced gel formation, and reduced structural defects.

6. Conclusions

This study examined how water-to-binder ratio, fine sand content, and NaOH concentration affect alkali-activated fly ash geopolymer. The main conclusions are as follows:

(1) Within the tested levels, the best overall mixture was obtained at a water-to-binder ratio of 0.30, fine sand content of 40%, and NaOH concentration of 12 mol/L. The maximum flexural and compressive strengths were 3.65 MPa and 17.98 MPa, respectively. NaOH concentration mainly controlled flexural strength, while the water-to-binder ratio had the strongest effect on compressive strength.

(2) The Random Forest model was useful for comparing factor effects and screening possible mix proportions, but it should not be treated as a validated prediction model. Cross-validation and model comparison showed that the current dataset was too small to support reliable general prediction.

(3) SEM, FTIR, and XRD results linked the strength changes to matrix densification, aluminosilicate network reorganization, and geopolymeric gel formation. Since the highest compressive strength was below 20 MPa, this pure fly ash geopolymer is more suitable for low- to moderate-strength applications. Further experiments are needed to verify the model-suggested mixtures.

Author Contributions: Conceptualization, Y.M.; methodology, Y.M.; software, Y.Z. and B.Z.; formal analysis, X.W.; resources, G.G.; data curation, X.W., Y.Z. and B.Z.; writing—original draft, X.W.; writing—review and editing, Y.M.; supervision, G.G. All authors have read and agreed to the published version of the manuscript.

Funding: This research was funded by the National Natural Science Foundation of China, grant number 52278184, under the project titled “Study on the Instability Mechanism and Design Basis for Global Stability of High Strength Steel Beam-columns under Combined Loads”.

Data Availability Statement: The original contributions presented in this study are included in the article. Further inquiries can be directed to the corresponding author.

Conflicts of Interest: The authors declare that they have no known competing financial interests or personal relationships that could have appeared to influence the work reported in this paper.

References

1. Nagalia, G.; Park, Y.; Abolmaali, A.; Aswath, P. Compressive Strength and Microstructural Properties of Fly Ash-Based Geopolymer Concrete. *J. Mater. Civ. Eng.* **2016**, *28*, 04016144. [CrossRef]
2. Davidovits, J. Geopolymers and geopolymeric materials. *J. Therm. Anal. Calorim.* **1989**, *35*, 429–441. [CrossRef]
3. Huang, H.; Guo, M.; Zhang, W.; Yang, S. Mechanical properties and microstructure of fly ash-slag base polymer concrete. *J. Harbin Inst. Technol.* **2022**, *54*, 74–84.
4. Wardhono, A.; Law, W.D.; Strano, A. The Strength of Alkali-activated Slag/fly Ash Mortar Blends at Ambient Temperature. *Procedia Eng.* **2015**, *125*, 650–656. [CrossRef]
5. Wang, Y.; Wang, Y.; Zhu, M.; Fang, C. Experimental study on the performance of low-doped fly ash-based polymer cementitious materials. *J. Shanghai Norm. Univ.* **2022**, *51*, 550–555.
6. Wong, L.S. Durability Performance of Geopolymer Concrete: A Review. *Polymers* **2022**, *14*, 868. [CrossRef] [PubMed]
7. Zhang, N.; Hedayat, A.; Sosa, H.G.B.; Cárdenas, J.J.G.; Álvarez, G.E.S.; Rivera, V.B.A. Damage evaluation and deformation behavior of mine tailing-based Geopolymer under uniaxial cyclic compression. *Ceram. Int.* **2021**, *47*, 10773–10785. [CrossRef]
8. Singh, S.; Aswath, M.; Ranganath, R. Effect of mechanical activation of red mud on the strength of geopolymer binder. *Constr. Build. Mater.* **2018**, *177*, 91–101. [CrossRef]
9. Peng, J.; Chen, W.; Dong, B.; Wang, Y. Alkali-activated sand washing slurry-based geopolymers: Mechanical strength, microstructure and environmental impact. *Constr. Build. Mater.* **2025**, *483*, 141779. [CrossRef]
10. Liu, Y.; Yuan, S.; Deng, K.; Cheng, X.; Zheng, Y.; Liu, X. Experimental study on strength characteristics and damage forms of NaOH-excited fly ash ground polymer. *Railw. Stand. Des.* **2025**, *69*, 79–86. [CrossRef]
11. He, B.; Zhang, W.; Tong, G.; Tang, X.; Liu, C. Compressive strength and microstructure of fly ash geopolymer. *China Powder Technol.* **2023**, *29*, 38–46. [CrossRef]
12. Liu, R.; Zhang, Y.; Wen, C.; Tang, J. Research on orthogonal experiment design and analysis method. *Exp. Technol. Manag.* **2010**, *27*, 52–55. [CrossRef]
13. Breiman, L. Random forests. *Mach. Learn.* **2001**, *45*, 5–32. [CrossRef]
14. Dao, D.V.; Ly, H.-B.; Trinh, S.H.; Le, T.-T.; Pham, B.T. Artificial intelligence approaches for prediction of compressive strength of geopolymer concrete. *Materials* **2019**, *12*, 983. [CrossRef] [PubMed]
15. Bin, F.; Hosseini, S.; Chen, J.; Samui, P.; Fattahi, H.; Armaghani, D.J. Proposing Optimized Random Forest Models for Predicting Compressive Strength of Geopolymer Composites. *Infrastructures* **2024**, *9*, 181. [CrossRef]
16. Khan, A.Q.; Naveed, M.H.; Rasheed, M.D.; Miao, P. Prediction of compressive strength of fly ash-based geopolymer concrete using supervised machine learning methods. *Arab. J. Sci. Eng.* **2024**, *49*, 4889–4904.
17. Zheng, S.; Liu, Z.; Huang, J.; Liu, L.; Jin, Q.; Zhang, Q.; Liu, Z.; Tang, G. A review of machine learning methods for geopolymer performance prediction: Linking data-driven models with physical insights. *J. Build. Eng.* **2025**, *114*, 114227. [CrossRef]
18. *GB/T 1596-2017*; Fly Ash Used for Cement and Concrete. Standardization Administration of China: Beijing, China, 2017.
19. *GB/T 17671-2021*; Test Method of Cement Mortar Strength (ISO Method). Standardization Administration of China: Beijing, China, 2021.
20. Matsimbe, J.; Dinka, M.; Olukanni, D.; Musonda, I. Fundamental machine learning algorithms and statistical models applied in strength prediction of geopolymers: A systematic review. *Discov. Appl. Sci.* **2024**, *6*, 538. [CrossRef]
21. Friedman, H.J. Greedy Function Approximation: A Gradient Boosting Machine. *Ann. Stat.* **2001**, *29*, 1189–1232. [CrossRef]
22. Sayash, K.; Arvind, N. Leakage and the reproducibility crisis in machine-learning-based science. *Patterns* **2023**, *4*, 100804. [CrossRef] [PubMed]
23. Varoquaux, G.; Raamana, P.R.; Engemann, D.A.; Hoyos-Idrobo, A.; Schwartz, Y.; Thirion, B. Assessing and tuning brain decoders: Cross-validation, caveats, and guidelines. *NeuroImage* **2017**, *145*, 166–179. [CrossRef] [PubMed]
24. Chen, T.; Guestrin, C. XGBoost: A Scalable Tree Boosting System. In *Proceedings of the 22nd ACM SIGKDD International Conference on Knowledge Discovery and Data Mining*; Association for Computing Machinery: New York, NY, USA, 2016.
25. Lv, Y.; Wang, C.; Han, W.; Li, X.; Peng, H. Study of the Mechanical Properties and Microstructure of Alkali-Activated Fly Ash–Slag Composite Cementitious Materials. *Polymers* **2023**, *15*, 1903. [CrossRef] [PubMed]
26. Liu, H.S.; Wang, Y.B.; Duan, Y.C.; Cai, G.H.; Zhang, Z.H.; Qiu, J.W. Study on mechanical properties and micro-mechanism of alkali-activated slag-fly ash geopolymer. *J. Beijing Univ. Technol.* **2026**, 1–13. Available online: https://link.cnki.net/urlid/11.2286.T.20260508.1021.002 (accessed on 23 June 2026).

27. Fernández-Jiménez, A.; Palomo, A.; Criado, M. Microstructure development of alkali-activated fly ash cement: A descriptive model. *Cem. Concr. Res.* **2004**, *35*, 1204–1209. [CrossRef]
28. Saeed, A.; Najm, H.M.; Hassan, A.; Sabri, M.M.S.; Qaidi, S.; Mashaan, N.S.; Ansari, K. Properties and Applications of Geopolymer Composites: A Review Study of Mechanical and Microstructural Properties. *Materials* **2022**, *15*, 8250. [CrossRef] [PubMed]
29. Gongga, D.Z.; Jiang, S.H.; Zhang, H.C. Study on strength and microstructure of fly ash-tailings geopolymer prepared under ambient conditions. *Brick-Tile* **2025**, *3*, 16–19. (In Chinese) [CrossRef]